Quantifying primary recrystallization from EBSD maps of partially recrystallized states of an IF steel

A Ayad, M Ramoul, A.D. D Rollett, F Wagner

Version of Record: https://www.sciencedirect.com/science/article/pii/S1044580320322440
Manuscript_a8d765a9ea32460d61942d5ed46b6cd6

Quantifying primary recrystallization from EBSD maps of partially recrystallized states of an IF steel

A. Ayad[1, 2], M. Ramoul[1], A.D. Rollett[3], F. Wagner[4, 5*]

[1]*Laboratoire Microstructures et Défauts dans les Matériaux, Univeristé Frères Mentouri Constantine 1, Route Ain El Bey, Constantine 25017, Algeria*

[2] *Département de Pharmacie, Faculté de Médecine, Université Salah Boubnider Constantine 3, Nouvelle ville Ali Mendjeli, Constantine 25005, Algeria.*

[3] *Department of Materials Science and Engineering, Carnegie Mellon University, Pittsburgh, PA 15213, USA*

[4] *LEM3 (UMR-CNRS 7239), Université de Lorraine -Metz, France.*

[5] *Laboratory of Excellence on Design of Alloy Metals for low-mAss Structures (Labex DAMAS), Université de Lorraine, France.*

*Corresponding author: francis.wagner@univ-lorraine.fr

Abstract: A set of IF steel specimens, at several stages of recrystallization, were subjected to EBSD analysis to provide data for a study of primary recrystallization. First, a criterion was defined for detecting the recrystallized grains that combines multiple parameters. The new approach pays particular attention to ensuring that reasonable recrystallized fractions are obtained in both the early and late stages of recrystallization. Using this to partition orientations maps into recrystallized and non-recrystallized grains, the distribution and density of nuclei, their correlation with EBSD parameters and stored energy, and their texture were determined. The evolution of the grain size distribution, microstructure and texture is then discussed in terms of the balance of the two main mechanisms (growth of the recrystallized grains into the deformed matrix and grain growth competition between already recrystallized grains) which occur during recrystallization.

Keywords: recrystallization texture, IF steel, EBSD, partitioning, partial recrystallization, nucleation, stored energy

1. Introduction

Heat treatment is an important aspect of the processing of metallic materials for optimizing the properties of the final product. Therefore, the study of recrystallization and its effect on the changes in the microstructures has given rise over the decades to a substantial literature that considers its various stages, i.e., recovery, nucleation, growth of recrystallized grains into the deformed matrix, grain growth competition [1-3]. This has been done using experimental data as well as models for a large variety of alloys [4-6]. Thanks to its development more than twenty years ago, EBSD (Electron Back Scattering Diffraction) has become an important tool for such studies. EBSD-based orientation maps are not only useful for determining the texture of a material but provide also a wealth of microstructural information such as grain size, grain boundary character, orientation gradients, and GND (Geometrically Necessary Dislocation) density [7]. Finding a way to obtain some insight into microstructure is especially important because the several mechanisms are not sequential but mainly simultaneous. At a given time during a heat treatment, some areas of a sample may be already recrystallized whereas some other areas are still recovered or even deformed. Although the literature is abundant, there are only few papers, for example [8-10], that provide quantitative data based on experiments, regarding questions such as nuclei density or nucleation rate or relative balance of the several mechanisms.

The goal of the present paper is to obtain information on primary recrystallization based on EBSD maps of partially recrystallized samples at several stages of recrystallization. The material used for this study is an interstitial-free (IF) steel. To achieve the goal, it is necessary to partition the maps into recrystallized and non-recrystallized grains, which is a process that itself has a substantial history [11-13]. Therefore, a new criterion was first developed for detecting the recrystallized grains that combines multiple parameters. By considering data from samples with low recrystallized fraction, the conditions of nucleation and the correlation

with stored energy are analyzed in detail. A specific misorientation parameter is defined to account for grain boundary mobility and analyze the various grain size distributions. Finally, the microstructure and texture evolution during primary recrystallization are discussed in terms of the balance between the main recrystallization mechanisms.

2. Materials and methods

The material used for this study was an IF steel whose composition is given in Table 1. The designation "IF" implies that the low levels of interstitials such as carbon and nitrogen are mostly sequestered in the form of carbo-nitrides.

Element	C	Mn	P	S	N	Si	Cu	Ni	Cr	Al	Ti	Fe
wt% $x10^{-3}$	8	196	4	10	31	4	7	18	14	41	97	Bal.

Table 1: chemical composition of the IF steel.

The as-received material was a 2.8 mm thick sheet after industrial warm rolling. Samples removed from this sheet were then cold rolled up to 75 % (thickness reduction) on a laboratory rolling mill and were then submitted to various heat treatments to generate partially recrystallized samples at various stages of recrystallization. Table 2 shows some characteristics of the samples selected for this study, all of which were cold rolled to a reduction in thickness of 75 %. S_0 is the deformed state, S_1 to S_5 correspond to partially recrystallized state whereas S_6 is fully recrystallized (after primary recrystallization and significant grain growth).

After standard metallographic preparation, EBSD measurements were made on a 6500F JEOL FEG SEM with an Oxford Instruments AZtec EBSD system. The post-processing of the raw data was done with the ATEX software [14].

Sample name	Heat Treatment Temperature (°C)	Heat Treatment Time (minutes)	EBSD map area (μm^2)	Step size for EBSD (μm)
S_0	-	-	66,849	0.15
S_1	630	5	44,771	0.15
S_2	620	15	125,829	0.40
S_3	625	60	225,500	0.50
S_4	630	30	29,708	0.15
S_5	630	45	267,307	0.40
S_6	800	300	240,500	0.50

Table 2: list of samples used in this study and conditions used for EBSD maps.

Basic characteristics of the EBSD maps are given in Table 2. For grain detection we used a threshold value of 5° for the misorientation angle between two adjacent pixels.

Figure 1 shows parts of the EBSD maps for the two extreme cases (cases with the least and the most recrystallized grains, i.e., samples S_1 and S_5.

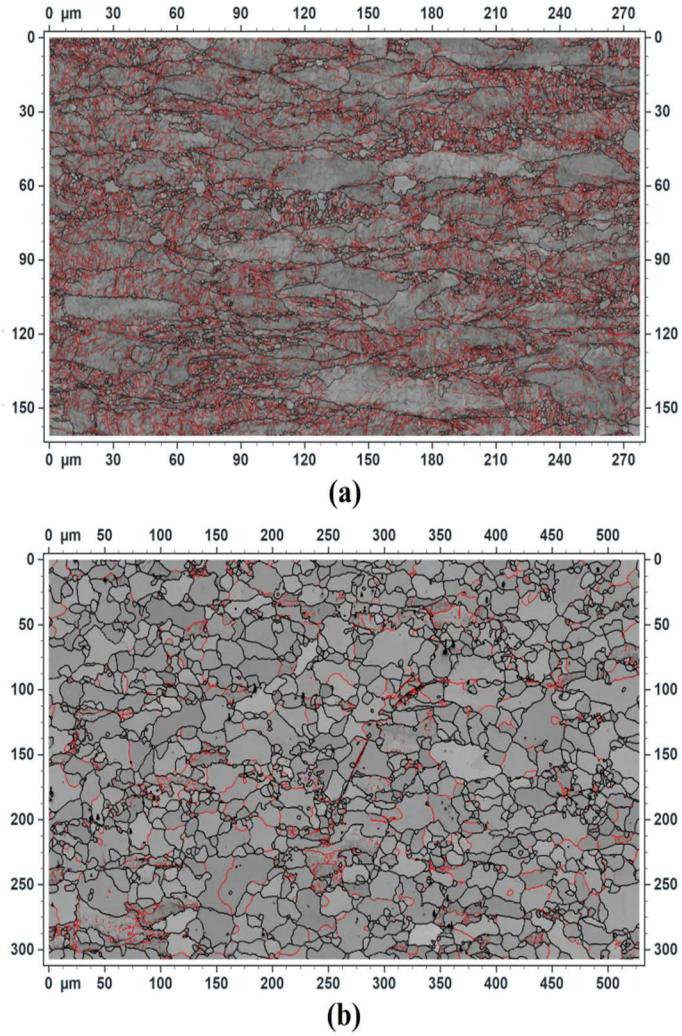

Figure 1: Band contrast map of samples S_1 (a) and S_5 (b) where grain boundaries (GBs) with a misorientation angle between 5° and 15° are in red and GBs with a misorientation over 15° are in black.

3. Detection of recrystallized grains

In partially recrystallized samples, it is essential to partition the grains into those which are already recrystallized in order to understand how recrystallization evolves. Such a procedure is always somewhat subjective because there is no precise definition for a recrystallized grain. There have been many parameters deduced from EBSD data for the discrimination of recrystallized grains and quantifying the recrystallization kinetics [7]. They are generally based on the quality of diffraction patterns (PQ) [15, 16] and measures of internal

misorientations such as: the Grain Orientation Spread (GOS) (see Eq. 1) [11-13, 17, 18], the Kernel Average Misorientation (KAM) (see Eq. 5) [19-21] and grain boundary analysis [22, 23]. Furthermore, the size and shape (i.e., aspect ratio) of recrystallized grains were taken into account in several cases [24-26]. The misorientation-based methods are more efficient than the PQ-based method for the identification of recrystallized grains. The latter is very sensitive to the contamination during sample preparation and depends on the measurement parameters [15, 27].

Several papers have suggested the use of GOS to detect recrystallized grains [11-13, 17, 28, 29].

For a grain numbered i, its grain orientation spread, GOS(i), is defined as

$$\mathrm{GOS(i)} = \frac{1}{n_i} \sum_{j=1}^{j=n_i} \omega\left(g_j, < g_i >\right) \qquad \text{Eq. 1}$$

where n_i is the number of pixels of the grain numbered i, j enumerates the pixels in this grain i and $\omega(g_j, <g_i>)$ is the misorientation angle between the orientation g_j of a pixel and the mean orientation $<g_i>$ of grain i.

For a set of N grains, a mean value, GOS, can be defined as

$$\mathrm{GOS} = \frac{1}{N} \sum_{i=1}^{i=N} \mathrm{GOS(i)} \qquad \text{Eq. 2}$$

The GOS is a measure of intragranular orientation gradient for long-range orientation consistency. However, the KAM is a pixel property, calculated as the average misorientation angle between that considered individual point and its neighbors (i.e., the kernel neighborhood) and can be used as the criterion for short range orientation consistency. The KAM is not adapted for identification of the recrystallized grains and grain boundaries between the recrystallized and deformed grains because of the kernel neighborhood value is

very sensitive to the step size. The GOS is considered to be the most successful tool for the identification of the recrystallized grains [24, 30, 31]. The reason for this can perhaps be found in the fundamental feature of primary recrystallization where long range boundary motion removes dislocation content which also removes (long range) orientation gradients.

Detection of the recrystallized grains is made using a limit value for GOS(i). A wide range of GOS threshold values from 1° to 3° has been used in the literature for various materials [18, 32] including IF steels [31, 33].

When one applies this criterion (GOS(i) < 2.5°) to the grains of the deformed specimen (sample S_0) one obtains 9,322 recrystallized grains! They represent 5.7 % of the map area and have a mean grain size of 0.7 μm. This is of course unacceptable for a purely deformed state. Even after decreasing the limit value for GOS(i), there remain small grains that are classified as recrystallized (for example 6,519 grains corresponding to 2.8 % of the map area and a mean grain size of 0.6 μm with the criterion GOS(i) < 1.5°).

It is therefore necessary to consider possible combinations of parameters to improve the detection of recrystallized grains. Several papers have proposed combinations between internal misorientations and other morphological criteria [31, 34, 35]. Wu and Juul Jensen [36] and Lin *et al*. [35] defined a recrystallized grain using three criteria: misorientation inside the grain smaller than a threshold value, larger than a certain size and at least partially surrounded (more than a defined number of pixels along the grain boundary) by high-angle boundaries (HABs) to the deformed matrix.

Kerisit *et al*. reported that analysis of the Kernel Average Misorientation maps coupled with that of the Grain Orientation Spread allows the discrimination of recrystallization and recovery [37]. Malta *et al*. [34] employed the GOS and KAM parameters combined with a minimum recrystallized grain size to determine the recrystallization kinetics and texture

evolution during recrystallization of a Nb-stabilized ferritic stainless steel. Gazder *et al*. [38, 39] partitioned EBSD maps into deformed, recovered and recrystallized fractions via a grain orientation spread threshold and an aspect ratio criterion. Furthermore, the recrystallized fraction was separated into newly nucleated and growing grain fractions based on a grain size criterion deduced from the frequency distribution of the recrystallized grain size. Using the GOS method and a grain size threshold for recrystallized grains discrimination, Kim *et al*. [31] reported that many small subgrains were misidentified as recrystallized because they have GOS values less than the limit value of 2.5°, for the deformed and the early stages of recrystallization; also many recrystallized grains were misidentified as deformed for the almost fully recrystallized state in an IF steel. In the parlance of data analytics, the rate of false positives and false negatives was unacceptably high. In order to reduce the misclassification of recrystallized grains, the authors proposed an adaptive threshold GOS that is adjusted according to the recrystallization stage: however, if one wants to track the early and the end stages of recrystallization, this method is strongly heuristic and unlikely to be transferable to other cases, just as they concluded.

With the objective of identifying the most significant parameters for recognizing recrystallized grains, we checked several parameters which can be calculated for each individual grain. The quantities considered were GOS(i), the 'normalized' value GOS(i)/D_i where D_i is the grain diameter, Ellip(i) the ellipticity of the grain and GND(i) the mean Geometrically Necessary Dislocation density in the grain. GND(j), associated to one pixel, is deduced from the orientation variation between this pixel and the neighbor ones [40-42]. GND(i) is the mean value for grain number i. It is provided as one of the output quantities obtained with the Atex software [14]. The ellipticity parameter, calculated for each grain, Ellip(i), is obtained by fitting an ellipse to each grain and calculating the quantity 1-b/a with a and b the length in the two main directions of the ellipse.

Table 3 shows the mean value of these parameters for all grains with at least 4 pixels (these quantities are considered as not meaningful for very small grains consisting of less than 4 pixels). In this table, the area fraction in % corresponds to the area of grains with at least 4 pixels.

Sample	No. grains ($\geq$ 4 pix.)	Area fraction (%)	$\langle D_i \rangle$ (µm)	$\langle GOS(i) \rangle$ (°)	$\langle GOS(i)/D_i \rangle$ (°/µm)	$\langle Ellip(i) \rangle$	$\langle GND(i) \rangle$ x10^{-14}(m^{-2})
S_0	12,819	94.6	2.5	2.18	2.12	0.44	7.03
S_1	7,170	97.8	2.8	1.53	1.23	0.36	4.12
S_2	17,298	95.8	2.9	2.09	1.14	0.40	3.16
S_3	12,990	97.0	4.6	1.78	0.64	0.42	1.77
S_4	1,603	99.1	4.8	1.11	0.65	0.36	2.38
S_5	3,938	98.9	9.2	0.65	0.21	0.36	0.74
S_6	757	99.6	20.1	0.54	0.05	0.30	0.61

Table 3: Number of grains, area fraction and mean parameters GOS, GOS/D, Ellip, GND density for all the grains with more than 3 pixels for the several samples.

The mean values GOS/D, GOS and GND density appear to be quite sensitive to the metallurgical state as already noted by previous authors [43, 44]. Because GND density is known to depend on the step size in the map [42], we searched for a combination of criteria based on GOS and GOS/D values. From our tests it appears that the criterion $GOS(i) < lim$ (2.5° for example) correctly identifies large grains which are very likely recrystallized but also selects many small grains that are likely not recrystallized. By contrast, the criterion $GOS(i)/D_i < lim$ (1°/µm for example) correctly identifies small grains that are probably recrystallized but also includes large grains which are not recrystallized. So the combination

of the two criteria appears to be a good solution for detecting the subpopulation of recrystallized grains.

A satisfactory combination should give, for the recrystallized fraction, a value close to 0 % for the deformed state (sample S_0) and a value close to 100 % for the fully recrystallized state (sample S_6). Table 4 shows the results obtained with the combination GOS(i) < 2.5° and $GOS(i)/D_i$ < 1°/µm, ignoring grains with less than 4 pixels. $\langle D \rangle_{ReX}$ is the mean grain size of the recrystallized grains and Rex-fraction is the recrystallized area fraction in %.

Sample	Number of ReX grains	ReX_fraction (%)	$\langle D \rangle_{ReX}$ (µm)
S_0	887	0.8	0.9
S_1	3,328	8.2	1.2
S_2	7,223	11.4	1.6
S_3	8,373	48.2	3.8
S_4	1,157	71.6	4.8
S_5	3,490	88.6	9.3
S_6	754	98.3	20.0

Table 4: number of recrystallized grains, recrystallized fraction and mean grain size of the recrystallized grains for the several samples using the described combination of criteria.

This combination of criteria appears to be satisfactory because it yields a very small area fraction of recrystallized grains (0.8 %) for the deformed state and a large one (98.3 %) for the fully recrystallized state. The other samples (S_1 to S_5) show correspondingly increasing recrystallized fractions.

Figure 2 shows the band contrast map for all the grains and the band contrast map for the grains detected as recrystallized in the case of the sample S_3 (recrystallized fraction of 48.2 %).

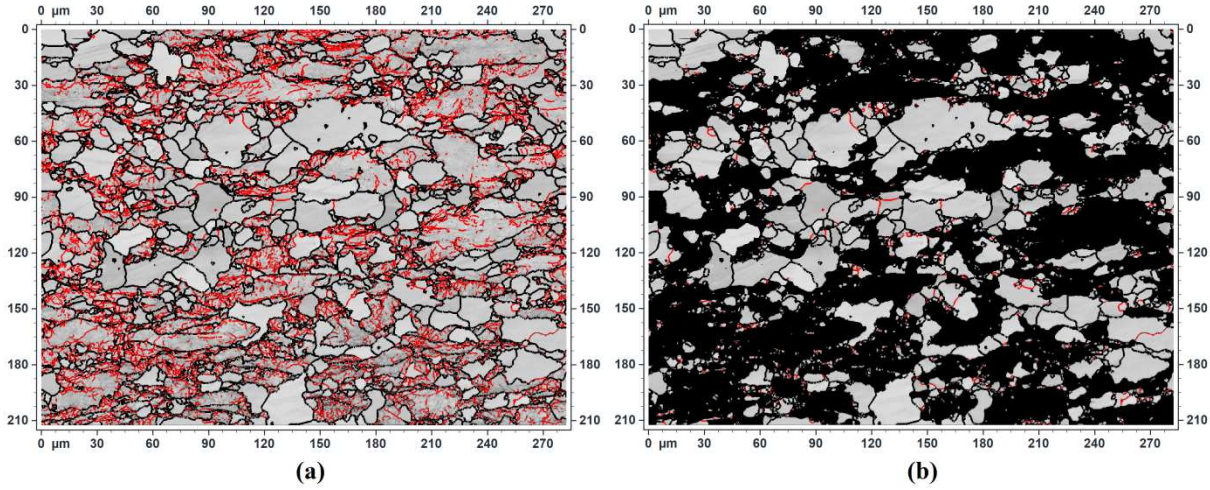

Figure 2: Band contrast map of sample S_3: a) for all the grains, b) restricted to the recrystallized grains detected with the described combination of criteria. Grain boundaries (GBs) with a misorientation angle between 5° and 15° are in red and GBs with a misorientation over 15° are in black.

This combination will be used in the following to select the recrystallized grains and discuss their properties.

4. ***Nucleation***

When considering the samples with low recrystallized fractions (8.2 % and 11.4 % for samples S_1 and S_2 respectively) it is possible to deduce some information on nucleation. Indeed, if one makes the reasonable assumption that each grain originates from a nucleus, one obtains the number of nuclei, their density and one can calculate the texture of the nuclei. For sample S_1, 3,471 recrystallized grains correspond to 3,471 nuclei and for sample S_2 one finds 7,223 nuclei. These numbers correspond then to a nucleus density of 0.08 /µm^2 for S_1

and 0.11 /μm^2 for S_2. This gives an estimate of the nucleus density which is useful for simulation or estimation of JMAK (Johnson–Mehl–Avrami–Kolmogorov) kinetics [1].

The spatial distribution of the nuclei is rather homogeneous. It is also possible to have a rough indication of the nucleation rate if one makes the crude assumption that the recrystallized grains grow with a constant growth speed in the deformed matrix. In this view the largest recrystallized grains come from the first appearing nuclei whereas the smallest recrystallized grains come from nuclei formed at the end of the heat treatment. Considering a grain with a diameter D_i, its growth time, tg_i, is then given by

$$D_i = 2\ v\ tg_i \qquad \text{Eq. 3}$$

where v is the growth speed in μm/mn. The growth speed v can be estimated by considering that, for the largest grain, its nucleus appears at the beginning of the heat treatment. The time t_i at which a nucleus number i appears is then

$$t_i = t_f - t_{gi} = t_f - D_i/2v \qquad \text{Eq. 4}$$

where t_f is the total time of the isothermal heat treatment.

Figure 3 shows, for the sample S_1, heat treated at 630 °C for 5 minutes, the grain size distribution for the 3,477 recrystallized grains (fraction in % versus diameter) and the time at which the 3,477 corresponding nuclei appear (fraction of nuclei in % versus time). For this sample the largest recrystallized grain has a diameter of 9.2 μm; this value was used to determine the grain growth speed according to Eq. 3 with $t_{gi}=t_f$ which leads to v=0.92 μm/mn.

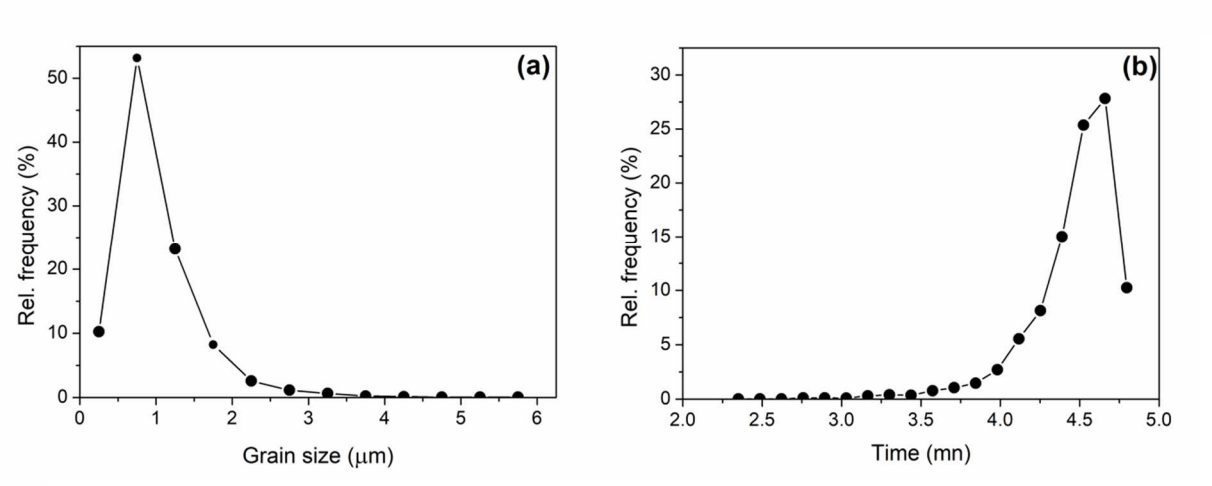

Figure 3: a) grain size distribution (fraction of grains in % versus diameter), b) fraction of nuclei in % versus time in minutes.

Figure 3b shows that most of the nuclei appear during a short period of time between 4 and 5 minutes of heat treatment. This indicates that the assumption 'site saturated' nucleation (i.e., all the nuclei appear at once), often used in modeling schemes of primary recrystallization, is quite acceptable.

The assumption that each recrystallized grain originates from a single nucleus also enables determination of the texture of the nuclei. The ODF (Orientation Density Function) of the nuclei is calculated using the following conditions: each nucleus has a weight equal to 1 and its orientation is the mean orientation of the corresponding recrystallized grain. Figure 4 shows, for the sample S_1, the partitioned ODF's obtained when considering all the grains, only the recrystallized grains and only the nuclei. Only the section ϕ_2=45° of the ODF where the main texture features appear is presented. Note that no sample symmetry is applied which requires the full range 0-360° for the first Euler angle ϕ_1.

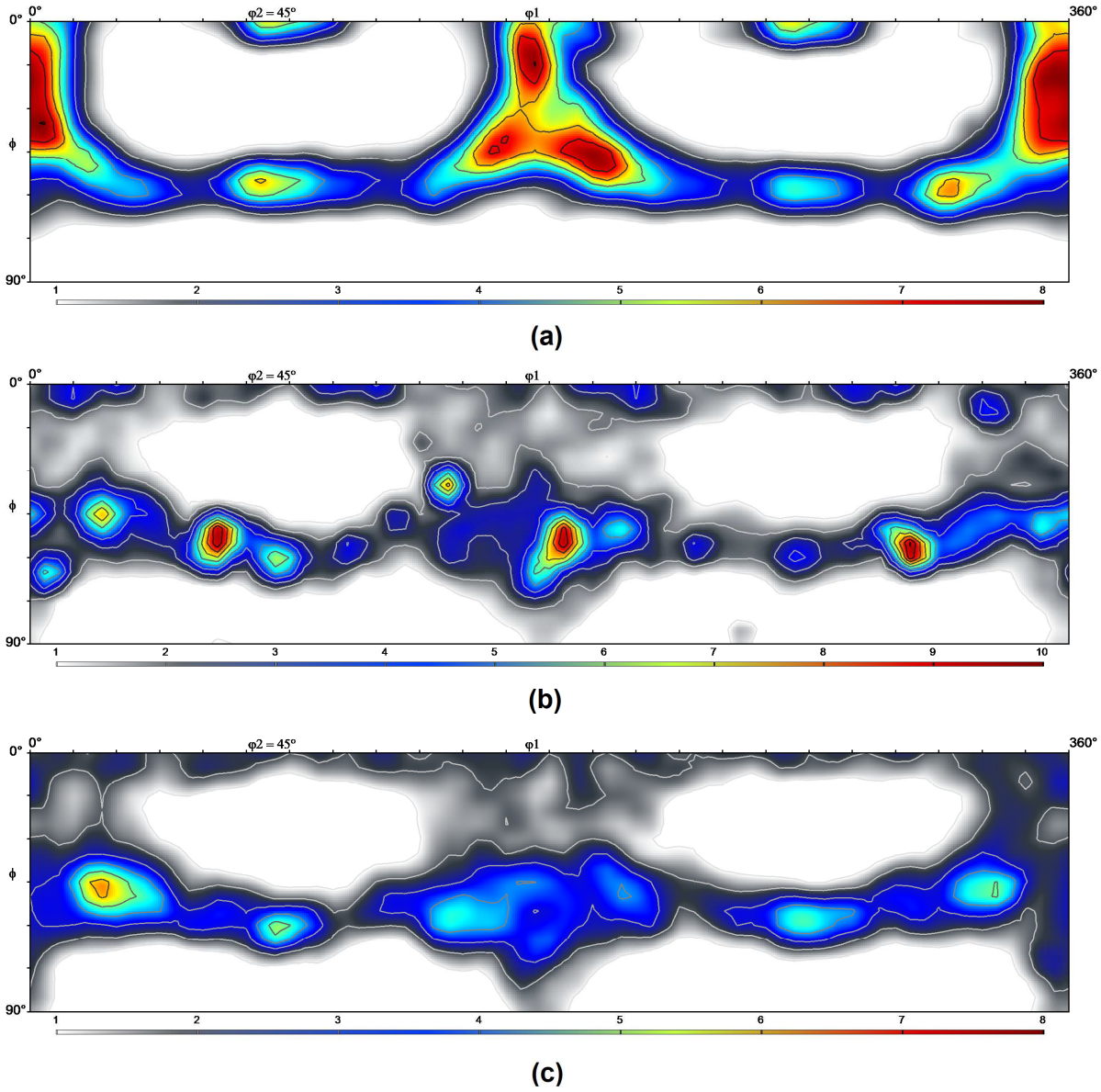

Figure 4: Section ϕ_2=45° of the ODF's for the sample S_1: a) all the grains, b) only recrystallized grains and c) nuclei.

When all the grains are taken into account (Fig. 4a), the texture is mainly a deformation texture with an alpha fiber and a weaker gamma fiber as the preferred orientations. When only recrystallized grains are included (Fig. 4b), the texture consists mainly of a gamma fiber with a peak around the orientation {111}<0 -1 1> , i.e. g={ϕ_1=60°, Φ=54.7°, ϕ_2=45°} (the 3 peaks are due to the cubic threefold crystal symmetry). The nuclei (Fig. 4c) exhibit a gamma fiber

texture type with a more homogeneous distribution along the gamma fiber compared to the recrystallized grains (Fig. 4b).

Globally the trend is clear for the texture. Primary recrystallization, at the early stage considered here, leads to disappearance of the alpha fiber and reinforcement along the gamma fiber because of the preferred orientation of the nuclei. This is in accordance with the trend classically observed in texture studies of low carbon steels [45-49].

5. ***Stored energy***

The stored energy in the deformed state plays an essential role for primary recrystallization because differences of stored energy between grains induce a driving pressure on grain boundaries. This even applies at very low deformation levels in strain-induced boundary migration [50]. It is therefore interesting to check if some parameters obtained from the EBSD map of a deformed sample can give information on its distribution. The number of parameters possibly linked with stored energy is quite limited. For this check, we have considered the quantities GND density and KAM (Kernel Average Misorientation) which can be calculated for each pixel of an EBSD map. For a pixel numbered i, the quantity KAM(i) is defined as

$$\mathrm{KAM(i)} = \frac{1}{\mathrm{nv_i}} \sum_{\mathrm{j=1}}^{\mathrm{j=nv_i}} \omega\left(\mathrm{g_i}, \mathrm{g_j}\right) \qquad \text{Eq. 5}$$

where nv_i is the number of neighbor pixels of the pixel numbered i, j enumerates the neighbor pixels and $\omega(g_i, g_j)$ is the misorientation angle between the orientation g_i of the pixel i and the orientation g_j of a neighbor pixel j. If a neighbor pixel j does not belong to the same grain as the pixel i, it is excluded from the sum. In our case where the EBSD map is displayed on a regular square grid we have chosen $nv_i=8$.

In our view a ‘successful’ nucleus, i.e., a nucleus that continues to grow as a recrystallized grain, is a small domain with few defects, embedded in an area with high stored energy (to have a high driving pressure on its borders) and having a significant misorientation with its vicinity (to have some mobility of its perimeter). Areas with high KAM values, or high GND density values, could therefore be the right places for nuclei. Note that although their definition is different, both quantities (KAM and GND density) are linked with orientation variation and are then expected to show, at least qualitatively, the same trend.

Both KAM and GND density have been calculated for all indexed pixels of the EBSD map of the deformed sample S_0. Then pixels with the highest values of KAM or GND density have been selected. The number of these selected pixels was fixed to correspond to the nuclei density (0.08 / μm^2) found previously. For the EBSD map area of sample S_1 (66,849 μm^2) one has then 5,347 pixels. The texture of these pixels were calculated and compared with the texture of the nuclei presented in the previous section. Figure 5 shows the section ϕ_2=45° of the ODF’s of the 5,347 pixels with the highest KAM and GND density values.

These ODF’s show similarities with the nuclei texture of Fig. 4c. To quantify the difference between an ODF calculated from the pixels with the highest KAM (or GND density) values and the ODF of the nuclei we have calculated the volume fraction of the difference function, V_Δ (see the definition in Appendix A). One obtains V_Δ = 21.5 % for KAM values and V_Δ = 29.1 % for GND values. If one makes the same calculation for the difference between the ODF of the nuclei and the one of the deformed state (without any filtering) one obtains a value V_Δ = 29.0 %. The texture obtained with KAM values is the closest with the one of nuclei with 78.5 % of the volume having the same orientations and 21.5 % having orientations which differ. Its compares also well with the texture of the pixels with the highest stored energy, where stored energy is calculated from a simulated deformation texture using a

CPFEM model [49]. Moreover, when considering the texture of the pixels with the lowest KAM values, for example, the 5 % of the pixels with the lowest values, there is also a reasonable agreement with the texture of the pixels with the lowest stored energy presented in [49]. KAM values appear then to be an acceptable indicator for stored energy, which is reasonable since KAM represents the local orientation gradients which in turn are present because of the GND content.

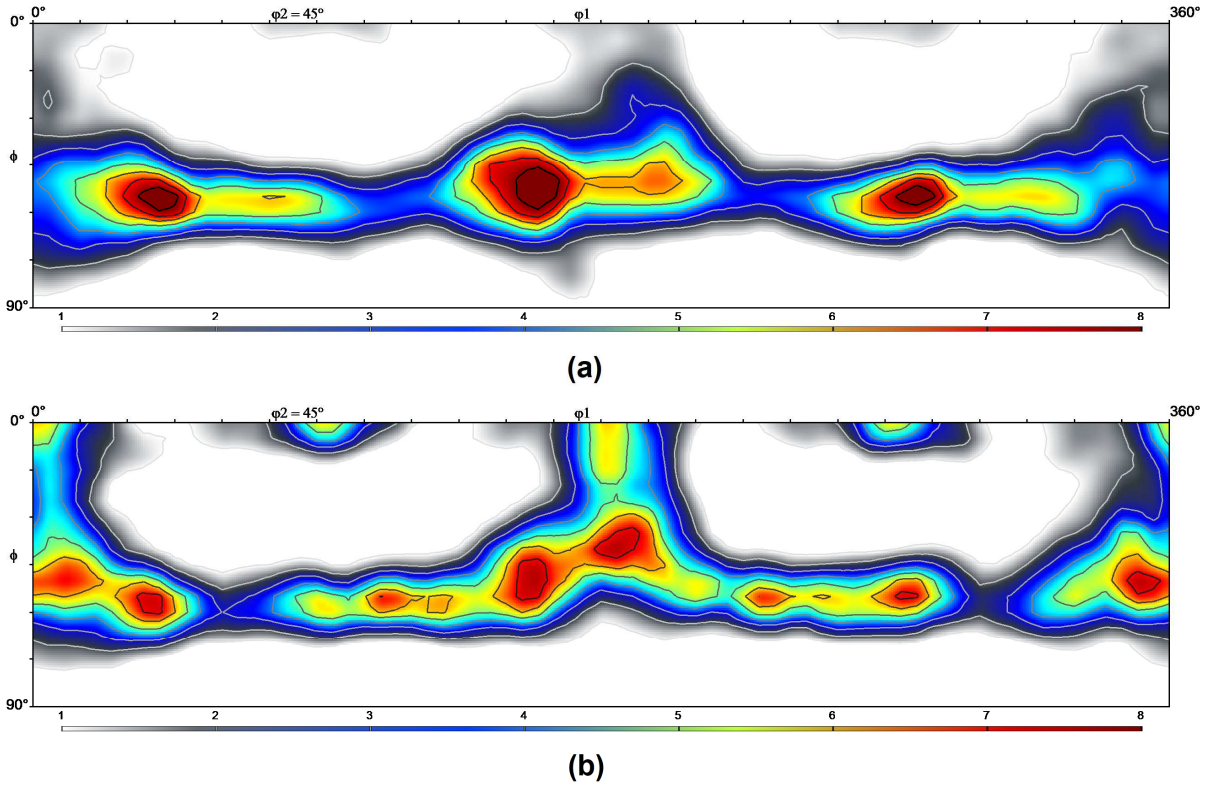

Figure 5: Section ϕ_2=45° of the ODF a) of the 5,347 pixels with the highest KAM values b) of the 5,347 pixels with the highest GND density values.

6. *Grain size distributions and Grain Boundary Mobility*

The detection of recrystallized grains from the several maps allows grain size distributions to be computed. Figure 6 shows the grain size distribution of the recrystallized grains for the five partially recrystallized samples S_1 to S_5. The most striking feature is that, in all the cases,

there is a long tail towards large grains. There are indeed a small number of grains much larger than the mean grain size.

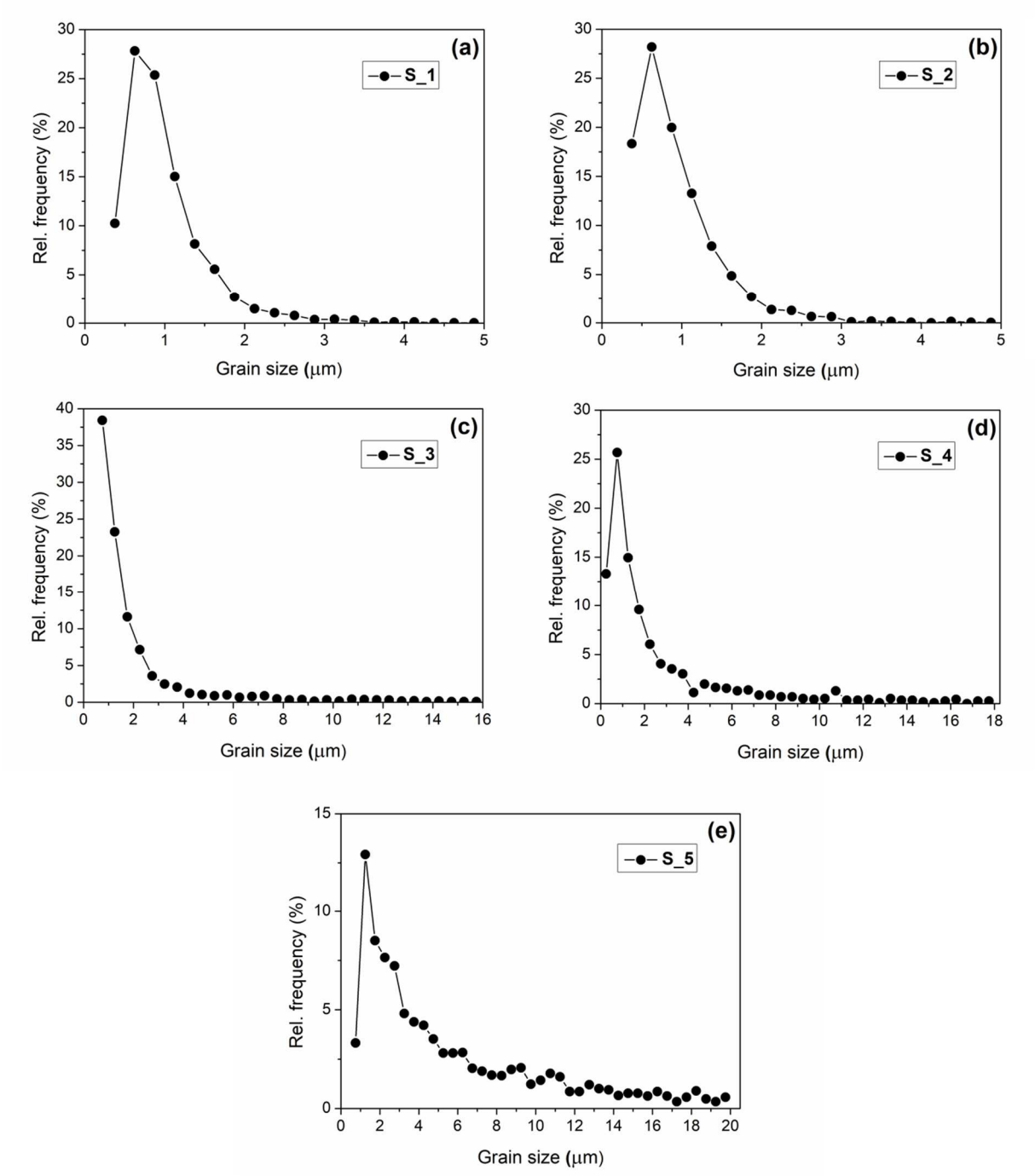

Figure 6: Grain size distribution (number of grains fraction in % versus grain diameter) of the recrystallized grains for: a) sample S_1, b) sample S_2, c) sample S_3, d) sample S_4 and e) sample S_5.

As emphasized previously, a nucleus must have mobile boundaries so that it can grow and become a recrystallized grain. We have checked some global characteristics of the grain boundaries of recrystallized grains, at several levels of recrystallization, to see if some specificities appear. In all the cases only a very small amount of CSL (Coincidence Site Lattice) boundaries exist which means that they do not play a significant role in the growth of the grains. To seek an explanation for observed grain size distributions, we calculated, for each grain, a grain vicinity misorientation parameter, denoted gvmp(i), defined as

$$\mathrm{gvmp(i)} = \frac{1}{\mathrm{L_i}} \sum_{\mathrm{j=1}}^{\mathrm{j=n_i}} \mathrm{L_{ij}}\ \omega\left(\mathrm{g_i}, \mathrm{g_j}\right) \qquad Eq.6$$

where L_i is the total length of GBs of the i^{th} grain, j numbers the grains in contact with the i^{th} grain, L_{ij} is the GB length between grain i and grain j and $\omega(g_i,g_j)$ is the misorientation angle between grains i and j. The parameter gvmp(i) is then in degrees. Note that it is a global parameter (i.e. one value per grain) which does not take into account the 'state' of the vicinity, i.e., whether a neighbor grain is already recrystallized or still deformed.

Figure 7 shows the distribution of this parameter for recrystallized grains and non-recrystallized ones for sample S_3 (48.2 % for the recrystallized fraction). There is only a very small shift or bias for the recrystallized grains to have larger misorientation angles.

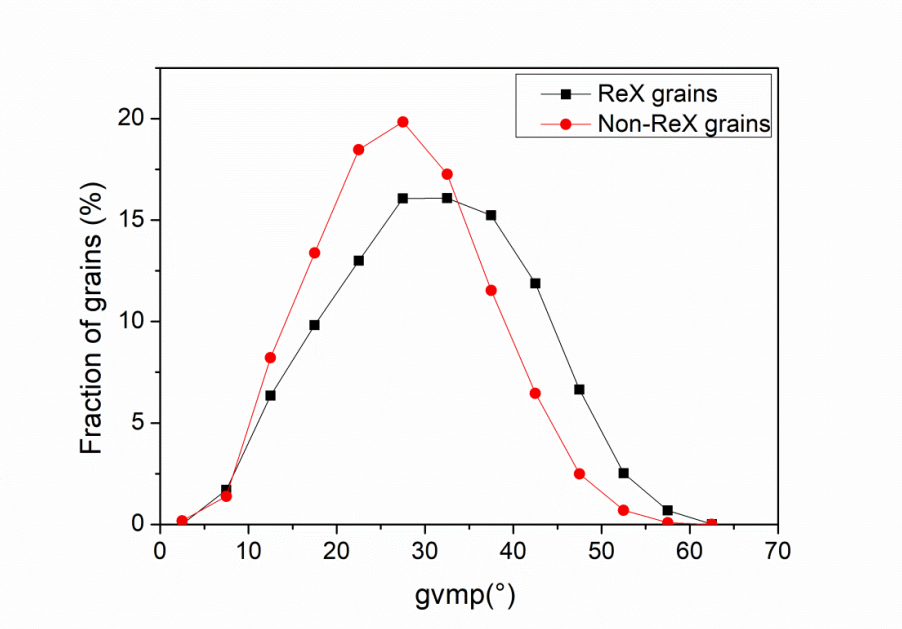

Figure 7: Fraction of grains (in %) versus the grain vicinity misorientation parameter (in degrees) in the case of sample S_3 for both the 8,373 recrystallized grains and the 4,617 non-recrystallized ones.

In Table 5 the mean value of the grain vicinity misorientation parameter is given for the three subpopulations (recrystallized grains, only the 20 largest recrystallized grains, and the not recrystallized grains) for the five partially recrystallized samples.

	S_1	S_2	S_3	S_4	S_5
ReX grains	28.2°	26.5°	30.8°	34.5°	36.4°
20 largest ReX grains	**37.1°**	**35.8°**	**39.7°**	**39.1°**	**35.8°**
Non-ReX grains	26.6°	24.7°	27.4°	29.5°	33.9°

Table 5: mean value of the grain vicinity misorientation parameter for the three grain subpopulations (recrystallized grains, 20 largest recrystallized grains, non-recrystallized grains) for samples S_1 to S_5.

The trend is similar for the samples S_1 to S_4. There is only a slight increase of this mean parameter for the recrystallized grains compared to the non-recrystallized ones. For the largest recrystallized grains (subpopulation made with the 20 largest recrystallized grains), however, the increase is significant with about 9° for the samples up to 48.2 % recrystallized. This difference disappears in sample S_5 (88.6 % recrystallization) where grain growth competition becomes an important mechanism.

Our results demonstrate at least a correlation between size and misorientation around a recrystallizing grain and opens the question: do the GBs with large misorientation angles have somehow a higher mobility? The question of GB mobility is very complex and data regarding its dependence on misorientation angle, *especially for medium and large angles*, are quite limited [51]. This suggests that consideration of whether higher mobilities occur at large misorientation angles is a meaningful question.

For our experiments, there are in fact several possible assumptions to explain the existence of a few large recrystallized grains. Indeed, these grains could be due to nuclei which appear very early and have then more time to grow or due to nuclei which were close to large deformed arrays with high stored energy or even a combination of both assumptions. This appears unlikely, however, because it implies that the nucleation rate is very slow in the early stages of recrystallization compared to later times.

Although our result about larger grain vicinity misorientation angles for the largest recrystallized grains is unlikely to have occurred just by chance, it is not yet possible to draw a clear conclusion on a higher intrinsic mobility of these particular GB's.

7. ***Evolution of microstructure and texture during primary recrystallization***

Three processes occur simultaneously during a heat treatment after plastic deformation: recovery, growth of recrystallized grains into the deformed matrix and grain growth

competition into the already recrystallized areas. Obviously the balance between these three processes evolves significantly along the heat treatment time. Recrystallization into the deformed areas and grain growth competition within clusters of recrystallized grains operate with quite different driving forces and have therefore different kinetics [1].

The grain size distribution and the mean grain size at the end of the primary recrystallization are then the result of these processes.

Figure 8 shows the evolution of the mean grain size of the recrystallized grains versus the recrystallized fraction (samples S_1 to S_5).

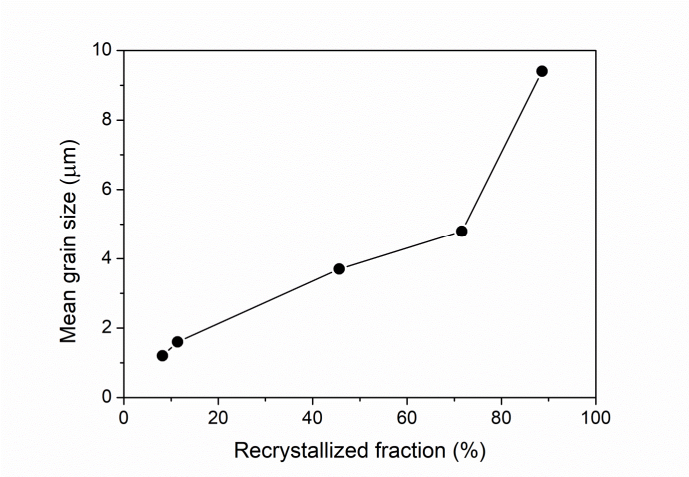

Figure 8: Evolution of the mean grain size of recrystallized grains (in microns) versus the recrystallized fraction (in %).

If one makes the assumptions that a) all the nuclei appear at once, b) that the grain growth into the deformed matrix has a constant speed and that c) there is no grain growth competition (2D model), such a curve is nearly linear except in the very beginning of the growth (between 0 % and 10 %).

Figure 8 shows clearly that, after a first linear part up to a recrystallized fraction around 50 %, there is a significant increase of the mean grain size. This is the indication that, after about 50 % recrystallized, grain growth competition becomes the dominant mechanism. This is also

confirmed if one considers the density of the recrystallized grains (number of recrystallized grains per micron square). This density is about 0.08 / μm^2 in the beginning (sample S_1 with 8.2 % recrystallization) and only 0.013 / μm^2 before the end (sample S_5 with 88.6 % recrystallization), which means that a large number of recrystallized grains (about 80 % of these grains) disappears, whereas some other (about 20 %) grow, mainly because of grain growth competition.

These results show that, if one wants to predict the evolution of grain size during primary recrystallization, starting from data in the deformed state, it is necessary to have a model that accounts for at least the two mechanisms, i.e., grain growth into the deformed matrix and grain growth competition as well as a correct balance of their importance.

In contrast to plastic deformation, primary recrystallization does not generate new orientations compared to the ones existing in the deformed matrix. Nuclei are assumed to be small 'clean' domains existing in the deformed matrix having given orientations. They define then, in the whole orientation space, a given orientation subspace. Along the primary recrystallization, the weights of the orientations in this subspace will increase or decrease according to the fact that some recrystallized grains develop or disappear.

Figure 9a shows the sections ϕ_2=45° of the ODF of the nuclei (defined above in section 3). The orientation subspace mentioned above is then the domain where this ODF is greater than 0, which is mainly centered on the gamma fiber.

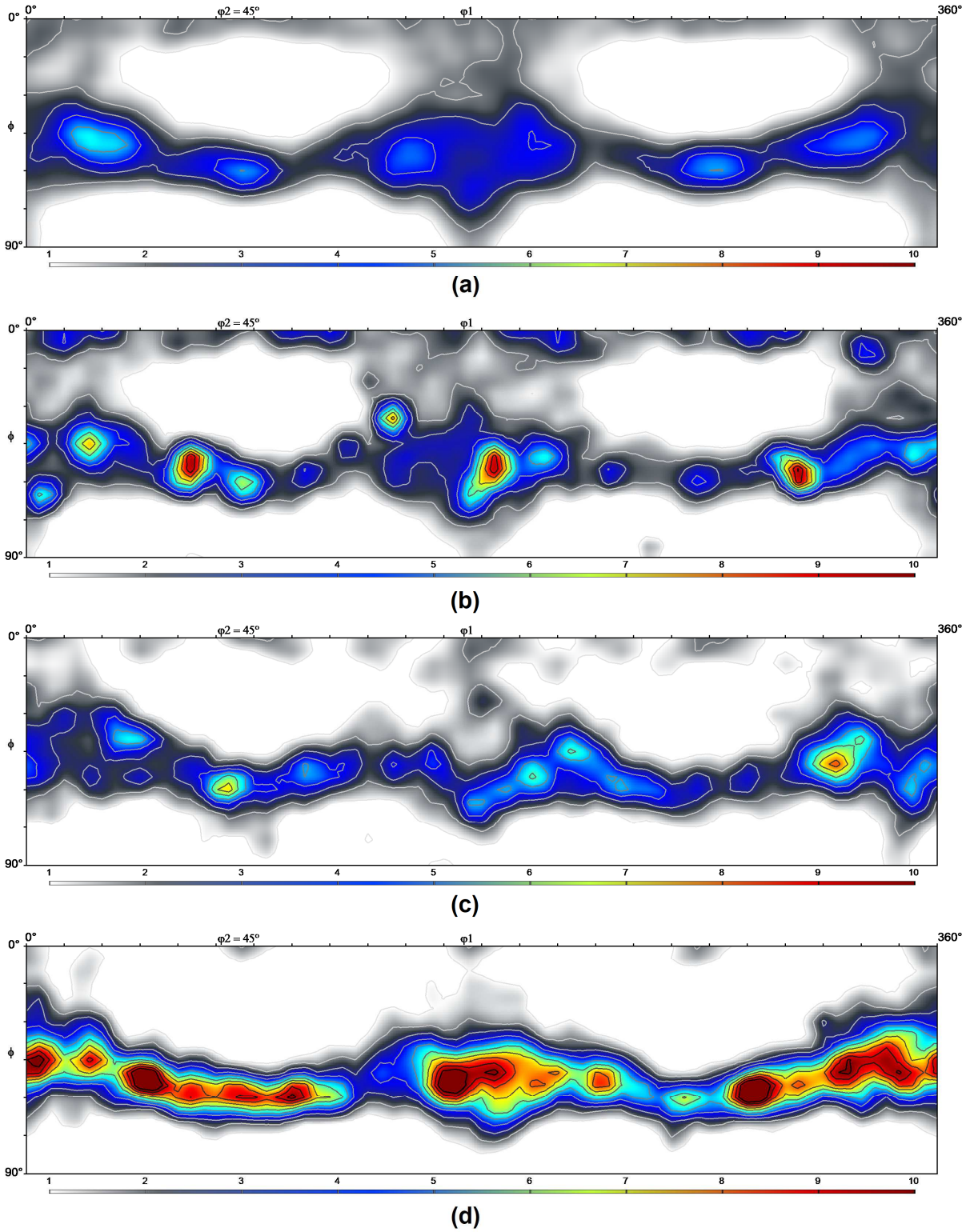

Figure 9: section ϕ_2=45° of the ODF for: a) the nuclei and for the recrystallized grains of samples: b) S_1 (8.2 % recrystallized fraction), c) S_2 (48.2 % recrystallized fraction) and d) S_5 (88.6 % recrystallized fraction).

During the first stage of primary recrystallization where the main mechanism is the growth of the recrystallized grains into the deformed matrix, a texture with mainly a gamma fiber builds up. After 8 % of recrystallization the gamma fiber has preferred orientations around (111)[0-11] (corresponding to the 3 orientations ϕ_1={60°, 180°, 300°}, with Φ =55°, ϕ_2=45°) and also a few orientations outside the gamma fiber (Fig. 9b). After 48 % of recrystallization the distribution along the gamma fiber is more uniform and the orientations outside the gamma fiber have weakened (Fig. 9c). One should note that, for these textures, the statistics are somewhat limited. Indeed, a small number of recrystallized grains, the largest ones, represent a large fraction of the recrystallized volume and thus a large part of the texture (for example, in the case of sample S_1 with 8 % recrystallization, the 100 largest recrystallized grains (over 3,328) represent 29 % of the recrystallized area).

During the second stage of primary recrystallization, where grain growth becomes important, the gamma fiber strengthens with reinforcement of several ideal orientations on this fiber (Fig.9d). Near the end of the primary recrystallization (recrystallized fraction close to 90 %) the remaining deformed grains (about 420 deformed grains in sample S_5) are concentrated in the alpha fiber with a peak around the ideal orientation (001)[110].

These results show that there is no simple rule for predicting the recrystallization texture as, for example, grains with a specific orientation will grow preferentially. The recrystallization texture at the end of the primary recrystallization is the consequence of topological effects (distribution of stored energy, nucleation and vicinity of growing recrystallized grains) and of the evolving balance between the mechanisms mentioned above.

8. *Conclusion*

A set of IF steel samples, at several stages of recrystallization, was processed and characterized by using EBSD maps with the objective of analyzing and quantifying several aspects of primary recrystallization.

i) Based on the need to partition orientation maps into subpopulations of recrystallized versus non-recrystallized grains, we show that a combination of three criteria (grain size larger than 3 pixels, GOS < 2.5° and GOS/D < 1°/μm) is an effective approach for this objective because reasonable values are obtained across the entire span of recrystallization.

ii) At low fractions recrystallized, by assuming that each recrystallized grain originates from a single nucleus, various data on nuclei become available. The number of nuclei was determined and their areal density was found to be in the range of 0.08 – 0.11 /μm^2. Moreover, with the admittedly crude assumption of a constant growth speed of recrystallized grains into the deformed matrix, it was shown that most of these nuclei appear in a very short time period. The ODF of nuclei showed that they have preferred orientations rather homogeneously distributed along the gamma fiber. This is also evidence for oriented nucleation.

iii) KAM and GND density were calculated for all the pixels of the deformed state. By calculating the textures associated with the pixels having the largest values for these quantities and comparing them to the nuclei texture, it was shown that the texture calculated from KAM values is the closest to that of the nuclei. KAM values appear then as an acceptable indicator for the stored energy distribution.

iv) The grain size distributions of the recrystallized grains show that, at the several stages of partial recrystallization, there are a few grains much larger than the mean grain size, i.e., the distributions are strongly right-skewed. A grain vicinity

misorientation parameter was defined to characterize the boundaries of the recrystallized grains. This parameter shows that the largest recrystallized grains have significantly larger misorientations on their boundaries except at the end of the primary recrystallization. Nevertheless, because there are several possible explanations for the existence of a few large recrystallized grains, it was not possible to conclude that the intrinsic mobility of GBs with high misorientation angles is larger.

v) Considering the mean grain size of recrystallized grains versus the recrystallized fraction showed that there are two regimes of microstructural evolution during recrystallization. Up to about 50 % of recrystallization, the growth of grains into the deformed matrix is the dominant mechanism whereas, over 50 %, grain growth competition becomes dominant. During this second period, many recrystallized grains disappear whereas the others grow quite significantly. The texture evolution is strongly related to the several described mechanisms. Nucleation selects an orientation subspace with preferred orientations along the gamma fiber, i.e., oriented nucleation occurs. During the first period (mainly growth into the deformed matrix) this gamma fiber strengthens slightly with a homogeneous distribution along the fiber. The grain growth competition that becomes important in the second period concentrates the texture on a few peaks along the gamma fiber.

Appendix A: quantification of texture difference

In order to compare two ODF's, $f_1(g)$ and $f_2(g)$, one can build the texture difference function $\Delta f(g)$ defined as:

$$\Delta f(g) = f_2(g) - f_1(g)$$

$\Delta f(g)$ has then positive and negative values; its integral over the whole orientation space is zero.

To characterize the 'intensity' of the difference with one number, one can use the volume fraction of the difference [52], denoted V_Δ, defined as:

$$V_\Delta = 0.5 \int_g \left| f_2(g) - f_1(g) \right| dg$$

(vertical bars mean absolute value; the integral is over the whole orientation space)

V_Δ is equal to 0 if the two functions $f_2(g)$ and $f_1(g)$ are identical and is equal to 1 if the two functions are completely different. V_Δ is the volume fraction of material having different orientations and can be multiplied by 100 to speak in % [52].

Acknowledgement

The authors thank Dr. B. Beausir and Dr. J.J. Fundenberger for including several facilities useful for this study into the ATEX software [14]. Two of the authors (A. A. and M. R.) express warm thanks to Pr. Nadjet ROUAG who gave strong support to develop this research topic at LMDM. These authors (A. A. and M. R.) also acknowledge financial support from the DGRSDT (MESRS-Algeria).

Data availability

The raw/processed data required to reproduce these findings cannot be shared at this time as the data also forms part of an ongoing study.

References

[1] F.J. Humphreys, G.S. Rohrer and A.D. Rollett, Recrystallization and Related Annealing Phenomena, 3rd edition, Elsevier, (2017).

[2] R. D. Doherty, D. A. Hughes, F. J. Humphreys, J. J. Jonas, D. Juul Jensen, M. E. Kassner, W. E. King, T. R. McNelley, H. J. McQueen and A. D. Rollett, Current issues in recrystallization: a review, Materials Science and Engineering A, Vol. 238, issue 2, (1997), p. 219-274

[3] Proceedings of the 7th International Conference on Recrystallization and Grain Growth (ReX&GG 2019), Ed. Leo A.I. Kestens Hadi Pirgazi Tuan Nguyen Minh Roumen H. Petrov, IOP Conf. Series: Journal of Physics: Conf. Series 1270 (2019)

[4] A. Brahme, J. Fridy, H. Weiland and A.D. Rollett, Modeling texture evolution during recrystallization in aluminum, Modelling and Simulation in Materials Science and Engineering, 17, issue 1, (2009), p 015005

[5] N. Peranio, Y.J. Li, F. Roters, D. Raabe, Microstructure and texture evolution in dual-phase steels: Competition between recovery, recrystallization, and phase transformation, Materials Sci. and Eng. A, 527, issue 16-17, (2010), p 4161-4168

[6] N. Dewobroto, N. Bozzolo, P. Barberis and F. Wagner, On the mechanisms governing the texture and microstructure evolution during static recrystallization and grain growth of low alloyed zirconium sheets (Zr702), Int. J. Mat. Res. (formely Zeitschrift für Metallkunde), 97, 6, (2006), p. 826-833

[7] A.J. Schwartz, M. Kumar, B.L. Adams, D.P. Field, Electron Backscatter Diffraction in Materials Science, 2nd ed., Springer, New York, (2009)

[8] I. Samajdar, B. Verlinden, P. Van Houtte, Development of recrystallization texture in IF-steel: an effort to explain developments in global texture from microtextural studies, Acta Materialia, 46, 8, (1998), p. 2751-2763. https://doi.org/10.1016/S1359-6454(97)00466-7.

[9] J-T. Park, J. A. Szpunar, Evolution of recrystallization texture in nonoriented electrical steels, Acta Materialia, 51, 11, (2003), p. 3037-3051. https://doi.org/10.1016/S1359-6454(03)00115-0.

[10] C. Haase, M. Kühbach, L. A. Barrales-Mora, S. L. Wong, F. Roters, D. A. Molodov, G. Gottstein, Recrystallization behavior of a high-manganese steel: Experiments and simulations, Acta Materialia, 100, (2015), p. 155-168. https://doi.org/10.1016/j.actamat.2015.08.057.

[11] D. P. Field, Quantification of partially recrystallized polycrystals using electron backscatter diffraction, Materials Science and Engineering A (Switzerland), 190, (1995), p.241-246

[12] A. D. Rollett, M. L. Taheri, and B. S. El-Dasher, Texture-Dependent Measurement of Recrystallization Kinetics Using Electron Backscatter Diffraction, Proc. Plasticity-02, A. Khan, ed. (2002) p. 42

[13] M. H. Alvi, S. W. Cheong, J. P. Suni, H. Weiland, and A. D. Rollett, Cube texture in hot-rolled aluminum alloy 1050 (AA1050) - nucleation and growth behavior, Acta materialia, 56, (2008), p. 3098-3108

[14] B. Beausir and J.J. Fundenberger, Analysis Tools for Electron and X-ray diffraction, ATEX - software, www.atex-software.eu, Université de Lorraine - Metz, (2017)

[15] J. Tarasiuk, P.H. Gerber, B. Bacroix, Estimation of recrystallized volume fraction from EBSD data. Acta Mater., 50, (2002), p. 1467–1477

[16] Y. Takayama, R. Hamano, T. Arakawa, H. Watanabe, Preferred orientation formation in surface layer of aluminum sheet subjected to friction roll surface processing and temperature gradient annealing, IOP Conf. Series: Journal of Physics: Conf. Series, 1270, (2019), p. 012028. doi:10.1088/1742-6596/1270/1/012028.

[17] M. Diehl, L. Kertsch, K. Traka, D. Helm, D. Raabe, Site-specific quasi in situ investigation of primary static recrystallization in a low carbon steel, Materials Science and Engineering: A, 755, (2019), p. 295-306. https://doi.org/10.1016/j.msea.2019.02.032.

[18] X.X. Wang, M. Zhan, P. F. Gao, P. Y. Ma, K. Yang, Y. D. Lei, Z. X. Li, Deformation mode dependent mechanism and kinetics of dynamic recrystallization in hot working of titanium alloy, Materials Science and Engineering: A 772, (2020), p. 138804. https://doi.org/10.1016/j.msea.2019.138804.

[19] M. Sanjari, M. Mehdi, Y. He, E. J. Hilinski, S. Yue, L. A. I. Kestens & A. Edrisy, Tracking the evolution of annealing textures from individual deformed grains in a cross-rolled non-oriented electrical steel, Metallurgical and Materials Transactions A,48, (2017), p. 6013–6026

[20] I. Kapoor, Y. Lan, A. Rijkenberg, Z. Li, V. Janik, Quasi in-situ analysis of geometrically necessary dislocation density in α-fibre and γ-fibre during static recrystallization in cold-rolled low-carbon Ti-V bearing microalloyed steel, Materials Characterization, 145, (2018), p. 686-696. https://doi.org/10.1016/j.matchar.2018.09.032.

[21] T. Ogawa, H. Dannoshita, Y. Adachi and K. Ushioda, Effect of initial microstructures prior to cold-rolling and intercritical annealing on ferrite recrystallization and ferriteto-austenite phase transformation in Nb bearing low-carbon steels, IOP Conf. Series: Journal of Physics: Conf. Series 1270, (2019), p. 012016. doi:10.1088/1742-6596/1270/1/012016.

[22] B. Chen, A. Yeh, J. Yeh, Effect of one-step recrystallization on the grain boundary evolution of CoCrFeMnNi high entropy alloy and its subsystems. Sci. Rep. 6, (2016), p. 22306. https://doi.org/10.1038/srep22306.

[23] X. Xu, J. Li, W. Li, Q. Liu, D. Liu, X. Wang, J. Wang, C. Shang, R.D.K. Misra, Experimental and theoretical study on static recrystallization of a low-density ferritic steel

containing 4 mass% aluminum, Materials & Design, 180, (2019), p.107924. https://doi.org/10.1016/j.matdes.2019.107924

[24] M. Zouar, N. Bozzolo, R. E. Loge, Mean field modelling of dynamic and post-dynamic recrystallization during hot deformation of Inconel718 in the absence of δ phase particles, Materials Science & Engineering A, 655, (2016), p. 408–424

[25] A. Nicolay, J.M. Franchet, J. Cormier, H. Mansour, M. De Graef, A. Seret, N. Bozzolo, Discrimination of dynamically and post-dynamically recrystallized grains based on EBSD data: application to Inconel 718, Journal of Microscopy, 273, 2, (2019), pp. 135–147. doi: 10.1111/jmi.12769.

[26] I. Kapoor, Y. Lan, A. Rijkenberg, G. West, Z. Li, V. Janik, Correlative analysis of interaction between recrystallization and precipitation during sub-critical annealing of cold-rolled low-carbon V and Ti–V bearing microalloyed steels, Materials Science and Engineering: A, 785, (2020), p. 139381. https://doi.org/10.1016/j.msea.2020.139381.

[27] S. Dziaszyk, E. J. Payton, F. Friedel, V. Marx & G. Eggeler, On the characterization of recrystallized fraction using electron backscatter diffraction: a direct comparison to local hardness in an IF steel using nanoindentation, Mater. Sci. Eng. A., 527, (2010), p. 7854–7864

[28] P.H. Gerber, J. Tarasiuk, R. Chiron and B. Bacroix, Estimation of the recrystallized volume fraction from local misorientation calculations, Archives of Metallurgy and Materials, 50, 3, (2005), p. 747-755

[29] D. Barbier, L. Germain, A. Hazotte, M. Gouné and A. Chbihi, Microstructures resulting from the interaction between ferrite recrystallization and austenite formation in dual-phase steels, J. Mater. Sci., 50, (2015), p. 374–381. Doi: 10.1007/s10853-014-8596-2.

[30] S.I. Wright, Proceedings of the 12th International Conference on Textures,1999, pp. 104–109.

[31] D.-K. Kim, W.-W. Park, H.W. Lee, S.-H. Kang & Y.-T. Im, Adaptive characterization of recrystallization kinetics in IF steel by electron backscatter diffraction, Journal of Microscopy, 252, 3, (2013), pp.204–216. doi:10.1111/jmi.12082

[32] M. Kulakov, J. Huang, M. Ntovas & S. Moturu, Microstructure evolution during hot deformation of REX734 austenitic stainless steel, Metallurgical and Materials Transactions A,51, (2020), p. 845–854

[33] J.-W. Park, H.-J. Jeong, S.-W. Jin, M.-J. Kim, K. Lee, J. J. Kim, S.-T. Hong, H. N. Han, Effect of electric current on recrystallization kinetics in interstitial free steel and AZ31 magnesium alloy, Materials Characterization, 133, (2017), P. 70-76. https://doi.org/10.1016/j.matchar.2017.09.021.

[34] P. O. Malta, D. S. Alves, A. O. Vasconcelos Ferreira, I. D. Moutinho, C. A. Pedroso Dias & D. B. Santos, Static recrystallization kinetics and crystallographic texture of Nb-stabilized ferritic stainless steel based on orientation imaging microscopy, Metallurgical and Materials Transaction A, 48, (2017), p. 1288–1309. Doi: 10.1007/s11661-016-3935-3

[35] F. Lin, Y. Zhang, W. Pantleon and D. Juul Jensen, Importance of non-uniform Boundary migration for recrystallization kinetics, Metall. and Ma.t Trans. A 49, (2018), 5246–5258. https://doi.org/10.1007/s11661-018-4846-2

[36] G.Wu and D. Juul Jensen, Automatic determination of recrystallization parameters based on EBSD mapping, Materials Characterization, 59, (2008), p.794 – 800

[37] C. Kerisit, S. Jacomet, N. Bozzolo, M. Houillon, W. Geslin, V. Llorca, R.E. Logé, Mesures des hétérogénéités de déformation du tantale déformé à froid et conséquences sur la recristallisation. MATERIAUX 2010 – 18-22 octobre 2010 – Nantes France, (2010)

[38] A.A. Gazder, M. Sanchez-Araiza, J.J. Jonas, E.V. Pereloma, Evolution of recrystallization texture in a 0.78 wt.% Cr extra-low-carbon steel after warm and cold rolling, Acta Mater., 59, 12, (2011) p. 4847-4865

[39] A.A. Gazder, A.A. Saleh, E.V. Pereloma, Microtexture analysis of cold-rolled and annealed twinning-induced plasticity steel, Scripta Materialia, 65, 6, (2011), p. 560–563

[40] B.S. El-Dasher, B.L. Adams, A. D. Rollett, Viewpoint: experimental recovery of geometrically necessary dislocation density in polycrystals, Scripta Mat., 48, 2, (2003), p.141-145

[41] W. Pantleon, Resolving the geometrically necessary dislocation content by conventional electron backscattering diffraction, Scripta Mat., 58, (2008), p.994-997

[42] D.P. Field, C.C. Merriman, N. Allain-Bonasso, F. Wagner, Quantification of Dislocation Structure Heterogeneity in Deformed Polycrystals by EBSD, Modelling and Simulation in Materials Science and Engineering, 20, 2, (2012), p. 12

[43] A. Ayad, N. Allain-Bonasso, N. Rouag and F. Wagner, Grain Orientation Spread values in IF steels after plastic deformation and recrystallization, ICOTOM 16, Déc. 2011, Materials Science Forum, 702-703, (2012), p. 269-272,

[44] N. Allain-Bonasso, F. Wagner, S. Berbenni and D.P. Field, A study of plastic heterogeneity in IF steel by EBSD, Mat. Sci. and Eng. A, 548, (2012), p. 56-63

[45] H.J. Bunge, Orientation Distribution Function of Crystallites in Cold-Rolled and Annealed Low-Carbon Steel Sheets, Physica Status Solidi, 26, issue 1, (1968), p.167-171

[46] L. Kestens and J.J. Jonas, Modeling texture change during the static recrystallization of interstitial free steels, Mettallurgical and Materials Transactions A, 27, issue 1, (1996), p. 155-164

[47] B. Hutchinson and D. Artymowicz, Mechanisms and Modeling of Microstructure/Texture Evolution in Intersttial-free Steel Sheets, ISIJ International, 41, n°6, (2001), p. 533-541

[48] K. Okuda and A. D. Rollett, Monte Carlo simulation of elongated recrystallized grains in steels, Computational Materials Science, 34, (2005), p.264-273

[49] D.-K. Kim, W. Woo, W.-W. Park, Y.-T. Im, A.D. Rollett, Mesoscopic coupled modeling of texture formation during recrystallization considering stored energy decomposition, Comp. Mat. Sci., 129, (2017), p. 55-65

[50] T.A. Benett, P.N. Kalu and A.D. Rollett, Strain-Induced Selective Growth in 1.5% Temper-Rolled Fe∼1%Si, Microscopy and Microanalysis, 17, issue 3, (2011), p. 362-367

[51] G. Gottstein and L. S. Schvindlerman, Grain Boundary Migration in Metals, 2nd edition, CRC Press, (2010)

[52] F. Wagner, N. Bozzolo, O. Van Landuyt and T. Grosdidier, Evolution of recrystallization texture and microstructure in low alloyed titanium sheets, Acta Mat., 50, (2002), p. 1245-1259